

Deep Multi-Task Learning for Malware Image Classification

Ahmed Bensaoud^{a,*}, Jugal Kalita^a

^aDepartment of Computer Science, University of Colorado Colorado Springs

ARTICLE INFO

Keywords:
 Malware Detection
 Multi-task Learning
 Malware Image
 Generative Adversarial Networks
 Mobile Malware
 Convolutional Neural Network

ABSTRACT

Malicious software is a pernicious global problem. A novel multi-task learning framework is proposed in this paper for malware image classification for accurate and fast malware detection. We generate bitmap (BMP) and (PNG) images from malware features, which we feed to a deep learning classifier. Our state-of-the-art multi-task learning approach has been tested on a new dataset, for which we have collected approximately 100,000 benign and malicious PE, APK, Mach-o, and ELF examples. Experiments with seven tasks tested with 4 activation functions, ReLU, LeakyReLU, PReLU, and ELU separately demonstrate that PReLU gives the highest accuracy of more than 99.87% on all tasks. Our model can effectively detect a variety of obfuscation methods like packing, encryption, and instruction overlapping, strengthening the beneficial claims of our model, in addition to achieving the state-of-art methods in terms of accuracy.

1. Introduction

The number of attacks on computers and computer networks is rising all over the world. Malicious software (or malware) is everywhere, with people trying to steal information from commercial or non-profit organizations and/or governments, and benefit politically, financially or otherwise. For example, a report from Cybersecurity & Infrastructure Security Agency (CISA) and Federal Bureau of Investigation (FBI) in May 2020 warned US organizations performing research on COVID-19 vaccines that foreign governments were attempting to hack into their system¹. McAfee Labs reported that 419 threats per minute were observed in Q1 2021, an increase of almost 6.33% over the previous quarter [1]. Malware is a prominent threat to smaller systems as well. Malware has also shown up in smartphones using Android and iOS systems due to the downloading of thousands of applications (apps) from the Internet. Every smartphone vendor has an application market for its OS, including Google Play, Blackberry App World, Windows Phone Marketplace (Microsoft Azure), and Apple Store. Apple apps for iOS devices such as iPhone, iPad, and iPod Touch can be installed only from the proprietary Apple App Store. If iOS users want to install apps that have not been approved by Apple, they need to remove the manufacturer's restrictions by jailbreaking. A jailbroken device allows users to gain full access to the root of the OS and gives users additional control. One of the top risks associated with jailbroken devices is higher susceptibility to malware. Android allows users to install from outside Google's app store, without jailbreaking. Android OS, which is open-source, is usually the first target of anyone who wants to develop malicious apps (see Fig. 1).

McAfee Labs Threats Report: June 2021

It is often in the third-party app repositories where

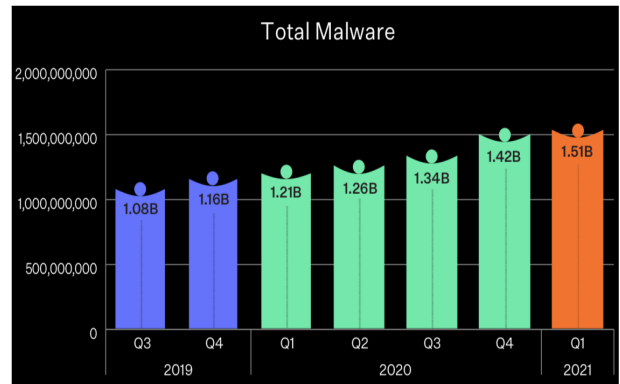


Figure 1: Total number of malware is increasing from quarter to quarter

malware authors upload their software with a goal to enable hackers to take control of a device by stealing passwords, or providing access to contacts. Thus, the development of intelligent techniques for malware detection is an urgent need. Unfortunately, malware classification is still challenging even though current state-of-the-art classifiers have achieved excellent results in general, especially in computer vision. To support efficient and effective malware classification, we propose a multi-task learning model in this paper.

Research on malware detection usually starts by extracting features from certain sections of malware files. In our research, we extract features from structural information in all files, in addition to performing dynamic analysis over the runtime behavior of the program files. We also extract features from the unpacked executables to detect obfuscation. To detect and classify malware using deep learning, we use all file sections instead of a specific section of the malware file like some previous efforts.

Multi-task learning (MTL) has been used successfully in areas such as computer vision, natural language processing and speech processing. For example, MTL has been extended to deep learning to improve the performance in computer vision. We employ multi-task

*Corresponding author:

 abensaou@uccs.edu (A. Bensaoud); jkalita@uccs.edu (J. Kalita)

ORCID(s):

¹<https://us-cert.cisa.gov/china>

learning for binary and multi-class malware image classification using seven submodels.

The availability of datasets to test and evaluate proposed malware detection models has been a bottleneck. That is why we create a large modern dataset as well. We make this dataset available to researchers.

Our contributions in this work are:

- We propose and implement a novel multi-task learning architecture for deep learning for malware classification.
- We create a benchmark color image dataset representing malware from portable executable, Android, ELF, Mac OS, and iOS files, and make it publicly available for the benefit of the research community².
- We conduct extensive experiments with various multi-task learning architectures for deep learning. Experimental results show that the proposed framework obtains excellent classification performance, achieving average accuracy of 99.97%. Our model is the state-of-the-art in malware classification.

The following is how we organize the paper’s overall structure. Section 2 discusses malware detection methods and multi-task learning. Section 3 details our methodology. Section 4 describes our method for generating image-like files from malware files to facilitate classification. Section 5 shows how we generate additional Mac OS malware samples using CycleGAN because the original numbers are small. Section 6 outlines our proposal of multi-task learning. Section 7 describes all datasets. In Section 8, we perform classification and evaluate the model. Section 9 presents experimental results. Finally, we provide conclusions and present the limitations of the study in Section 10.

2. Related work

This section discusses the related work regarding malware detection approaches, malware visualization and classification based on deep learning, and multi-task learning.

2.1. Malware detection

To defend computer systems from malware, we need to detect malware before it affects the computer systems. Three traditional approaches have been used to detect malware: Signature-based detection, Heuristic detection, and Behavior-based detection. These methods have a number of advantages and disadvantages. 1) Signature-based detection efficiently identifies known malware using pattern matching, but is unable to identify unknown malware since malware can change its characteristics, producing a new signature that signature-based detection cannot identify. 2) Heuristic detection can identify known and unknown malware, but this method

can lead to high error rates for false-positives and false-negatives. 3) Behavior-based malware detection approaches observe the behavior and purpose of a suspicious file. This approach needs resources and time to execute and monitor the behavior of the suspicious file.

Machine learning models have also been applied in malware detection. Supervised machine learning algorithms such as naive Bayes (NB), C4.5 decision tree variant (J48), random forests (RF), support vector machines (SVM), sequential minimal optimization (SMO), k-nearest neighbors (KNN), multilayer perceptron (MLP), and simple logistic regression (SLR) have been used to detect malware. Ucci et al. [2] surveyed malware analysis using machine learning techniques and discussed various features that have been used by researchers to improve malware detection systems. Recently, researchers have also attempted to detect malware using deep learning. They have indicated that basic deep learning models perform well in malware analysis. In addition, researchers have shown that it is possible to build a combination of two or more models to strengthen the outcomes.

Alzaylaee et al. [3] proposed DL-Droid, a deep learning system to detect malicious Android applications through dynamic analysis. They evaluated the model using 31,125 Android applications, 420 static and dynamic features, and compared performance with existing DL-based frameworks. Dynamic features on DL-Droid achieved up to a 97.8% detection rate and 99.6% with dynamic and static features. Darabian et al. [4] used static and dynamic analysis for system calls of Portable Executable (PE) samples of cryptomining applications. They collected system call data and then fed into the deep learning models—LSTM, Attention-based LSTM, and Convolutional Neural Networks (CNNs). Their models achieved 95% accuracy rate in static analysis on opcode and accuracy rate of 99% in dynamic analysis on system calls. Deep learning models for static and dynamic analysis of malware have been explored, producing promising results to detect obfuscated malware [5].

Malware authors develop obfuscation techniques such as packaging, shuffling, encryption, and tokenization to make it harder to detect, thus, elude anti-malware engines [6]. The current obfuscation detection techniques for Android applications perform poorly. A recent survey on Android malware detection using the latest deep learning algorithms has investigated the challenges and analyzed the results of obfuscation detection systems[7]. In addition, detection of Linux malware is also still in its infancy, but such malware is already using IoT devices of different negative behaviors and tricks. Unfortunately, analyzing ELF files is quite difficult since Linux runs in devices of all kinds from a really small tier masters to really large servers [8].

2.2. Malware Image

Malware executable can be represented as a matrix of hexadecimal or binary strings and converted to a form which can be thought of as an image. To create a new malware, malware authors usually add to or change the code in old malware. Thus, when viewed as an im-

²<https://github.com/abensaou-uccs/Colorado-MalColorImg>

age, one can easily visualize small adds or changes in various sections of the file structure. Nataraj et al. [9] first proposed a technique to convert malware into images, transforming the raw bytecode PE files to greyscale image data where a pixel is represented by a byte. Vasan et al. [10] performed image-based malware classification using an ensemble of CNN architectures to detect packed and unpacked malware files. The approach used two pre-trained models, VGG16 and ResNet-50, which were fine-tuned for classification of malware images. The approach achieved more than 99% accuracy for unpacked malware and over 98% accuracy for packed malware.

Su et al. [11] converted malware binary in IoT environments to image and used a light-weight convolutional neural network to classify malware families. Their model achieved 94.0% accuracy for goodware and DDoS malware, and 81.8% for goodware and two powerful malware families.

Ni et al. [12] proposed the MCSC (Malware Classification using SimHash and CNN) model which hashed decompiled malware code and converted it to grayscale images, and then trained CNNs for classification. Their model achieved an average accuracy of 98.86% on a malware dataset of 10,805 samples.

Bensaoud et al. [13] used six deep learning models for malware classification. Three of these are past winners of the ISVLCRC contest: VGG16, Inception V3, and ResNet50, and the other three models are CNN-SVM, GRU-SVM, and MLP-SVM, which enhance neural models with support vector machines (SVM). They trained all models on the Malimg dataset [9], and the results indicate that the Inception-V3 model achieved a high test accuracy of 99.24% among all compared work.

Naeem et al. [14] converted APK files to color images and then fed them to a DCNN model. The model achieved 97.81% accuracy on the Leopard Mobile malware dataset³ and 98.47% accuracy on a Windows dataset⁴.

Kalash et al. [15] proposed a CNN-based architecture to classify malware samples. They performed experiments on two datasets, Malimg and Microsoft malware. The method achieved 98.52% on 9339 Malimg malware samples from 25 malware families and 99.97% on 21,741 Microsoft malware samples⁵.

Mercaldo and Santone [16] proposed a platform for a static approach for the detection of malicious samples using supervised deep learning. They gathered a set of features from gray-scale images to build several classifiers to identify the belonging malware family and the variant inside the family. The family detection model obtained an accuracy of 93.50% and variant detection obtained an average accuracy of 95.80%.

2.3. Multi-Task Learning

Often learning how to perform several tasks simultaneously helps perform one or more of the tasks bet-

ter than learning to perform tasks individually. We use multi-task learning in our work since it can be used for binary and multi-class malware classification simultaneously. It can also improve the performance on several related datasets.

In multi-task learning, multiple related tasks are learned jointly, and useful information is shared among related tasks. Each task benefits from other tasks producing better results for one or more trained tasks. Several related tasks are learned jointly from a shared dataset. There are two approaches, 1) Hard parameter sharing, where hidden layers are shared by all tasks, with different output layers as shown in Fig. 2. 2) Soft parameter sharing, where different tasks have their own networks, but parameters are made similar by regularization, and the output layers are different, as shown in Fig. 3. One important advantage of hard parameter sharing is that it reduces the number of parameters in the model since the same feature space is used by all closely related tasks. In addition, it performs as a regularizer that reduces the risk of overfitting and makes the model architecture compact for efficient training. Moreover, hard sharing parameters use a single shared representation and then connect to multiple tasks, with each task represented as a submodule. Meyerson and Miikkulainen [17] showed that combining gradients from each task improves learning. Zhang et al. [18] proposed a deep learning-based multi-task learning approach to predict network-wide traffic speed, using a set of hard parameters and Bayesian optimization.

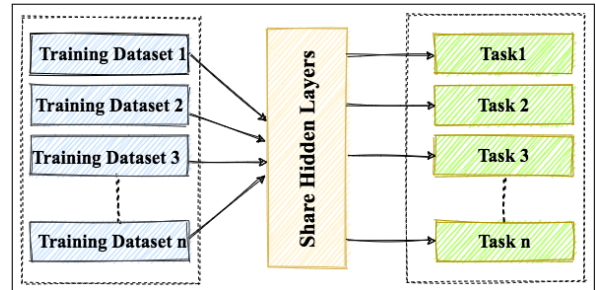


Figure 2: Hard parameter sharing for multi-task learning (MTL)

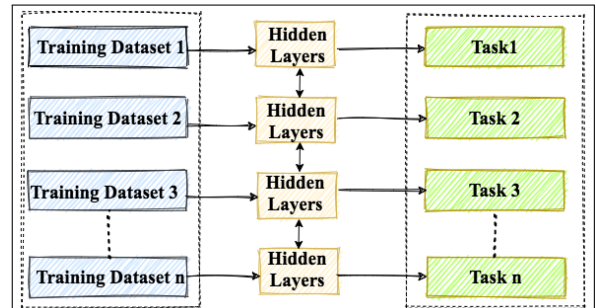


Figure 3: Soft parameter sharing for multi-task learning (MTL)

Many MTL methods have been proposed to solve

³<https://sites.google.com/site/nckuikm/home>

⁴<https://vision.ece.ucsb.edu/research/>

signal-processing-malware-analysis

⁵<https://www.kaggle.com/c/malware-classification>

classification problems in computer vision. Gkioxari et al. [19] applied a convolutional neural networks for the tasks of pose prediction and action classification of people in unconstrained images. Zhao et al. [20] proposed an attribute hierarchy based multi-task learning (AHMLT) approach for fine-grained image classification on CUB-200-2011 [21] and Cars-196 datasets [22]. Their approach achieved the best classification performance at the time. Bell et al. [23] built an image product recognition system called GrokNet, using a multi-task learning approach, matching the accuracy of a previous state-of-the-art Facebook product recognition system. Yu et al. [24] constructed BDD100K, a large-scale driving video dataset with 100K videos and 10 tasks for image recognition algorithms on autonomous driving. They created a benchmark for heterogeneous multitask learning and studied how to solve the tasks together. The results showed interesting findings about allocating the annotation budgets in multitask learning. Chen et al. [25] proposed a multi-task learning based salient region detection method by fusing spatial and temporal features. The model learned a two-stream Bayesian model by integrating spatial and temporal features in a unified multi-task learning framework, outperforming previous methods. Wang et al. [26] used a semi-supervised learning technique to address the missing visual field measurement label problem in the training set, and built a multi-task learning network to explore the relationship between the functional and structural changes in glaucoma and classify optical coherence tomography (OCT) images into glaucoma and normal. They achieved good results for the automated diagnosis system. Dorado-Moreno et al. [27] proposed and evaluated a multi-task deep neural network architecture for predicting Wind Power Ramps Events (WPRES) in three different classes. They modified the Adam optimization algorithm for imbalanced data for the misclassified class. Their model achieved very good performance for all the classes.

3. Methodology

We apply a multi-task learning model to learn from several malware datasets. The datasets are built with malware for PE Windows, APK Android, ELF Linux, and Mach-O for MacOS X. We extract features from sections in each malware file and convert them to RGB images and feed them to our model.

3.1. PE Malware

The Portable Executable (PE) file is the structure of all executable files (EXE) and Dynamic Link Libraries (DLL) that can be loaded and executed on any version of Microsoft Windows. The structure of a PE file includes DOS Header, PE Header, Optional Header, Sections Table, and sections that contain Code, Import, and Data. A PE file relies on several DLL files for execution, and each DLL is related to other DLLs to implement a certain task. The actual executable has different sections such as .text, .data, .idata, .edata, .rsrc, .reloc,

.bss, and .debug, as shown in Fig. 4.

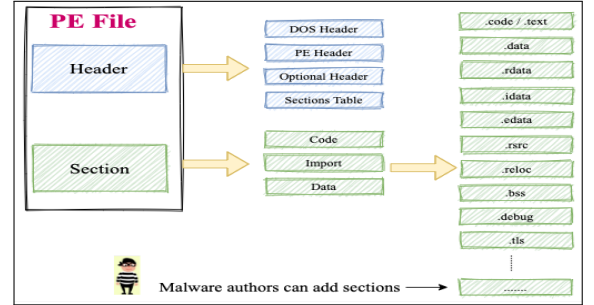


Figure 4: PE file structure

3.2. Executable and Linkable Format (ELF)

An executable file on Linux is structured using the ELF syntax. There are two different file formats, dynamic libraries (*.so) and object files (*.o) [28]. Low focus on Linux threat detection by the antivirus industry motivates many malware writers to attack this operating system. Researchers have shown that ELF malware is quite complicated, demonstrating that malware authors put in a lot of effort in creating Linux malware. Examples of Linux malware are Rootkits, Exploits, and Backdoors, that DDoS attack malware usually use. The latest and most dangerous ELF malware is a combination of various individual types. We extract all ELF features from the samples: ELF headers, program header tables, code, data, section names, and section header tables. We use PwnTools, which is a convenient Python library to extract the hexadecimal form of malware ELF files.

3.3. MacOS X and iSO Malware

The core of any operating system is known as the kernel. In MacOS and iOS, the name of the kernel is called Mach kernel, and its executable format is named Mach-O file. There are several types of Mach-O files, such as .o, .dylib and .bundle extensions. We download the iOS App Store Package .ipa file from iTunes and remove digital rights management (DRM) protection to get decrypted executable. In addition, we collect malware samples from VirusTotal⁶ and Contagio⁷. It is hard to find open source malware repositories from MacOS. This is the reason why we use the CycleGAN technique to generate more Mach-O malware. For benign Mach-O files, we collect open source programs. The dataset consists of 5000 malware samples and 2000 benign samples.

The Mach-O malware features are extracted from all section headers, load commands, and segments by parsing the file structures using a Python script, and are converted to hexadecimal as shown in Fig. 5.

3.4. Android Malware

Android Package (APK) is a compressed (ZIP) bundle of files used by Android OS for mobile apps. We ex-

⁶<https://www.virustotal.com>

⁷<http://contagiadump.blogspot.com>

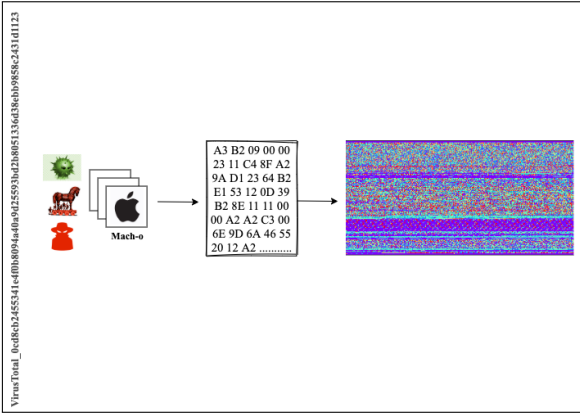


Figure 5: Converting MacOS malware Mach-o file to image

tract the contents of APK files: `AndroidManifest.xml`, `classes.dex` (interpreted by Dalvik VM), `META-INF` and resource files. The `AndroidManifest.xml` file describes information in the APK file like the package name, app components, the manifest permissions needed to access protected resources and hardware components. We parse both the Android manifest file and `classes.dex` to extract the features. We convert all these files to hexadecimal, merge them, and generate the RGB images using Android library in Python as shown in Fig. 6.

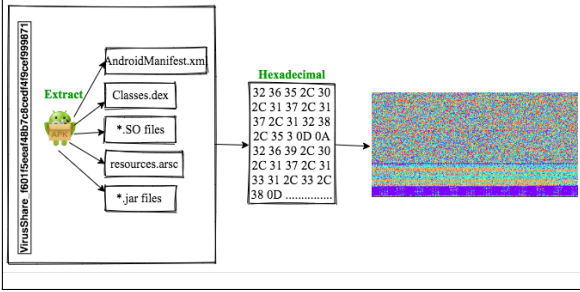


Figure 6: Converting Android malware APK file to image

3.5. Unpacking Malware

We consider malware packing since malware authors obfuscate, compress and encrypt malicious code via executable packing, making it hard to detect malware [29]. We unpack malware using the state-of-the-art packing detection and packing classification tool PEiD [30]. The goal of unpacking malware is to merge the static and dynamic features in one image.

3.6. Assembling Code to Image

We convert the malware samples to assembly code by using a popular disassembler, IDA Pro⁸. IDA Pro decodes binary machine code into readable assembly language code as shown in Fig. 7.

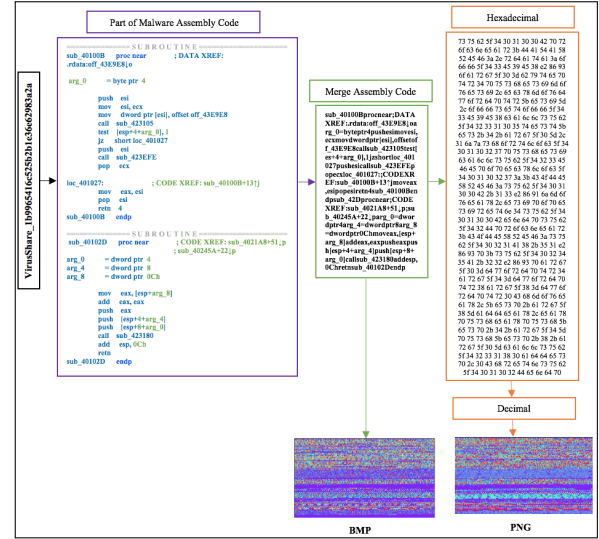


Figure 7: Converting sequence of assembly instructions of the malware to Image

4. Generating Images

An image is a set of numbers that record the intensity of red, green, and blue at every pixel location in an image in a grid format of pixels. Each pixel in the image can be represented by a vector in three primary color spaces, red (R), green (G), and blue (B). Let

$$P_i = \begin{bmatrix} R_i \\ G_i \\ B_i \end{bmatrix}$$

where P_i is the i th pixel of the image, $1 \leq i \leq S$, where the size of the image is S . The mean value (μ) and the standard deviation (σ) represent global features of the image and are calculated as follows:

$$\mu = \frac{1}{S} \sum_{n=1}^S P_i,$$

$$\sigma = \sqrt{\frac{1}{1-S} \sum_{n=1}^S (P_i - \mu)^2}.$$

Fig. 8 shows how an RGB pixel is stored in the image format. For instance, a pixel can be stored in up to 48 bits, with sixteen bits per channel.

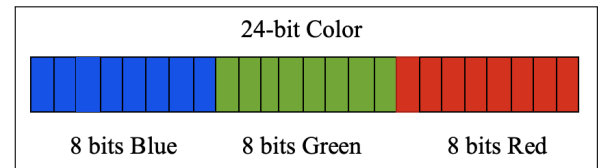


Figure 8: PNG 24 bits image in RGB color

4.1. Malware Image Generation

Files that look like images can be generated from a malware file in either raster or vector form. Raster

images store the data as a grid of pixels. The most common raster image formats include Windows Bitmap (BMP), Joint Photographic Experts Group (JPEG), and Portable Network Graphics (PNG) images formats. On the other hand, vector format images are made up of objects based on geometric features such as circles, lines, polygons, rectangles, and curves. The most common vector images are Scalable Vector Graphics (SVG) and Vector Markup Language (VML). In this paper, we use BMP and PNG raster image formats since there is no need to scale up the images that SVG and VML vector formats allow.

In an RGB image, each channel's values go from 0 to 255, assuming each color channel is represented with 8 bits or a byte. The maximum number 8 bits can represent is 255 and the lowest is 0. Therefore, there are 256 possible intensities per color channel. For example, to represent a pixel of the color Sunglow, the values of RGB are 250 for a lot of red, 200 for a lot of green, and 62 for a little blue. The computer stores them as Red: 11111010, Green: 11001000, and Blue: 11111000, using 24 binary digits to represent such a pixel. We can represent the same color Sunglow using only six hexadecimal digits as FA C8 3E, which is a lot shorter than binary. A wide range of application software graphics packages express colors using hexadecimal codes. The image file can be stored in uncompressed (lossless) or compressed (lossy) formats.

In addition, rows can be padded if necessary. For example, if we have an image size 17×17 , each row needs 17 times 3 = 51 bytes. We can test if the rows need padding or not by finding the modulo of row by 4 (51 MOD 4 = 3). The result of the modulo gives us how many padded rows are needed.

4.2. Bitmap (BMP) and Portable Network Graphics (PNG)

The bitmap (map or array of bits) file format is used to store two-dimensional color images [31]. BMP files are uncompressed. They are also larger than other format images such as JPEG, GIF, and PNG. The bitmap file format has sections which contain file header, information header, data color table, and pixel values. A bitmap contains precise information about each and every pixel. BMP is the best type of input for malware classification using image files since the format does not use compression. A key reason for using large file sizes is to keep all malware features. On the other hand, the PNG file format uses lossless compression to store raster images in smaller space. Similar to BMP, PNG also keeps all malware features.

When we generated a BMP or PNG image from malware file as shown in Fig. 9, we had to consider padding since there is a gap between row width and length of the image. For example, if the image is 51×51 with depth 24-bit, each row needs $51 \times 3 = 153$ bytes. We also compressed the BMP image using Run Length Encoding, which is a lossless compression approach. We use this approach since it reduces the size of the malware BMP image with no loss of information (see

Figs. 10 and 11).

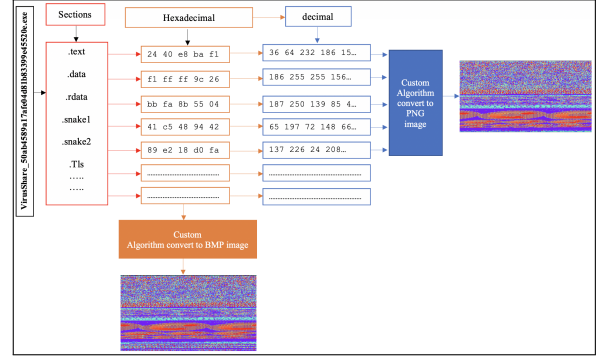


Figure 9: Converting malware to BMP and PNG Image

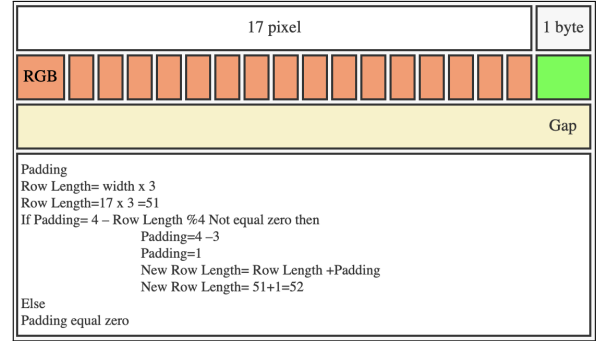


Figure 10: Padding Gap

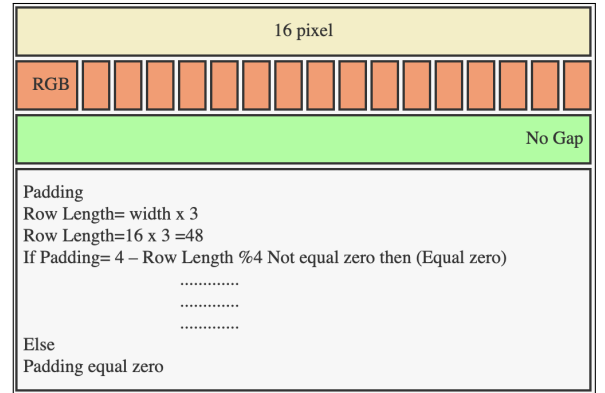


Figure 11: No Padding Gap

5. Generative Adversarial Networks

Generative Adversarial Networks (GANs) [32] recently have achieved impressive results in image generation [33, 34, 35]. A GAN consists of a couple of neural networks that compete with each other. One is called the generator and the other the discriminator. The generator network tries to generate realistic samples that have never been seen before. The discriminator network tries to tell whether its inputs are real or fake. A GAN can be used to generate fake malware images. Specifically, it will improve the learning efficiency of

our model by increasing the number of examples on what to train.

Many applications of GANs in computer vision have achieved impressive performance such as SRGAN [36], pix2pix [37], CycleGAN [38], DiscoGAN [39], DualGAN [40] and StarGAN [41]. Among these, CycleGAN is quite proficient in generating adversarial examples. It has achieved state-of-the-art results in image-to-image translation. CycleGAN has been applied to generate artificial training data if sufficient amount of real training data is not available. We use CycleGAN since we do not have enough Mac OS malware samples. Cycle-GAN is used to translate malware to benign images while simultaneously supervising an inverse benign to malware transformation model.

5.1. CycleGAN

We use CycleGAN to map benign(x) to malware(y), and also map back to benign as shown in Fig 12. The CycleGAN model is used to convert Mac OS malware file to image using two mappings $G_{XY} : X \mapsto Y$ and $G_{YX} : Y \mapsto X$, which fulfill the following constraints:

- **Generator G** : $X \mapsto Y$: translates images from X to Y (malware to benign)
- **Generator F** : $Y \mapsto X$: translates images from Y to X (benign to malware)
- **Discriminator DX** : scores how real an image X looks (Does this image look like benign?)
- **Discriminator DY** : scores how real an image Y looks like (Does this image look like a malware?)

5.1.1. Objective function of CycleGAN

As described above, the model relies on improving both the generator and discriminator. We have two losses, one is adversarial Loss corresponding to the GAN and the second is Cycle Consistency Loss which computes how close the reconstructed image is to the original image.

• Adversarial Loss

Adversarial loss is applied to both our mappings of generators and discriminators. The generator attempts to minimize the adversarial loss, and the discriminator attempts to maximize it. This adversarial loss shown below.

$$\begin{aligned} \mathcal{L}_{(G, D_y, X, Y)} = & \mathbb{E}_{y \sim p_{data(y)}} [\log(D_y(y))] + \\ & \mathbb{E}_{x \sim p_{data(x)}} [\log(1 - D_y(G(x)))] \end{aligned} \quad (1)$$

The equation above is to compute D_x loss where $p_{data(y)}$ is the set of all malware image samples (represents the data distributions of y).

$$\begin{aligned} \mathcal{L}_{(G, D_x, Y, X)} = & \mathbb{E}_{x \sim p_{data(x)}} [\log(D_x(G(x)))] + \\ & \mathbb{E}_{y \sim p_{data(y)}} [\log(1 - D_x(G(y)))] \end{aligned} \quad (2)$$

The equation above is to compute D_Y loss where $p_{data(x)}$ is the set of all benign image samples (represents the data distributions of x),

• Cycle Consistency Loss

CycleGAN employs a forward and backward cycle consistency loss. The cycle consistency loss generates the content of the image efficiently while the image is translating. Cycle Consistency is computed as the difference between real and reconstructed images. In addition, two-cycle consistency losses guarantee that image that is transferred from one domain A to domain B, and back again will be the same. The formulation of cycle consistency is shown below:

$$\begin{aligned} \mathcal{L}_{(G, F)} = & \mathbb{E}_{x \sim p_{data(x)}} [\|F(G(x)) - x\|_1] + \\ & \mathbb{E}_{y \sim p_{data(y)}} [\|F(G(y)) - y\|_1] \end{aligned} \quad (3)$$

where, $\|F(G(x)) - x\|_1$ is the forward cycle consistency loss, and $\|F(G(y)) - y\|_1$ is the backward cycle consistency loss

5.1.2. Combined Objective Function

The combined objective function is the summation of adversarial loss when converting malware to benign and benign to malware and their corresponding cycle consistency losses.

$$\mathcal{L}_{(G, F, D_x, D_y)} = \mathcal{L}_{(G, D_y, Y, X)} + \mathcal{L}_{(G, D_x, X, Y)} + \mathcal{L}_{(G, F)}$$

5.1.3. Optimization

CycleGAN performs optimization corresponding to: $\mathcal{L}_{(G, F, D_x, D_y)}$ to come up with the generator that generates malware from benign and benign from malware.

$$G^*, F^* = \arg \min_{G, F} \max_{D_x, D_y} \mathcal{L}(G, F, D_x, D_y)$$

6. Our Multi-task Learning Model

Several malware image samples are large, more than 1 megabyte. Therefore, large-scale malware image classification is a challenging task. In fact, when we used the state-of-the-art CNN models such as InceptionV3 [42], VGG19 [43], and ResNet [44] for malware image binary classification, the accuracy rate came out very low. The issue is that the computational cost for large-scale image classification becomes unacceptable. We want a model with a capacity to learn from 100,000 malware images. We also need high-performance computing systems with GPUs or TPUs for classifying large public malware image repositories. MTL can be used to save both time and memory needed by a learning system. How can we build an architecture for multi-task learning for large-scale malware images? To answer this question, we first create multiple deep CNNs

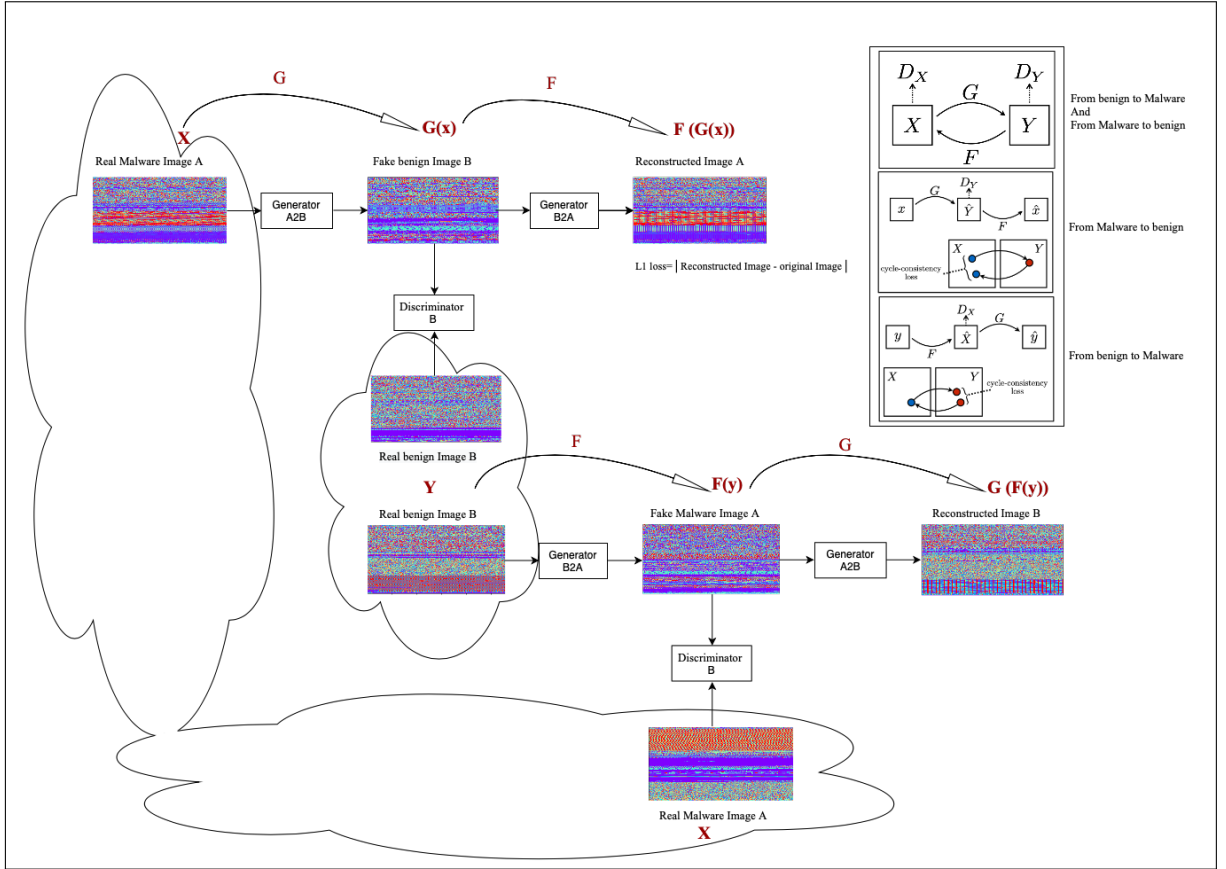


Figure 12: Generating malware images using CycleGAN

for deep multi-task learning to develop joint training for different combination of tasks. Second, we design a network that can take input with different sizes of malware images. In particular, the width and height for input malware images are determined by the malware file size. We designed a MTL model consisting of seven classification tasks for malware image classification. As shown in Fig. 13, our deep multi-task learning algorithm is developed for joint training of multiple deep CNNs. Each CNN model contains 5 convolutional layers with PReLU activation function. The first four convolutional layers are followed by a max-pooling layers with a stride of 2 and the fifth convolutional layer is followed by two fully connected (FC) layers with PReLU activation function. Each FC layer consists of 1024 neurons as shown in Fig. 14.

6.1. Convolutional neural network (CNN) layers

A CNN is able to scale up to hundreds of layers with improving performance. In our model, we created large 9x9 filter for the first layer to shrink a large malware image to a moderate size. Besides, when we designed the model, we kept adding layers until the model over-fit at layer 12. Therefore, we designed the model with 11 layers. In addition, the feature map size should be large at the beginning and then a decrease. It is an acceptable assumption since a large malware image needs high resolution feature maps.

6.2. Activations

An activation function maps a node's inputs to its output. We use four different activation functions that lead to different levels of performance in our model.

6.2.1. Rectified Linear Unit (ReLU)

ReLU is the default activation function in deep learning. We use ReLU since it allows faster training time. It has been successfully applied in various state-of-the-art deep neural networks [45, 46]. It is defined as $f(x) = \max(0, x)$, where x is the input of the activation function [47]. In other words,

$$f(x) = \begin{cases} 0 & \text{for } x < 0, \\ x & \text{for } x \geq 0. \end{cases}$$

6.2.2. LeakyReLU

LeakyReLU replaces the negative part of the ReLU with a linear function by using fixed negative slope of 0.01 [48]. LeakyReLU is defined as:

$$f(x) = \begin{cases} 0.01x & \text{for } x < 0, \\ x & \text{for } x \geq 0. \end{cases}$$

We experimented with LeakyReLU since it has been used in many Kaggle competition projects and achieved high performance [49].

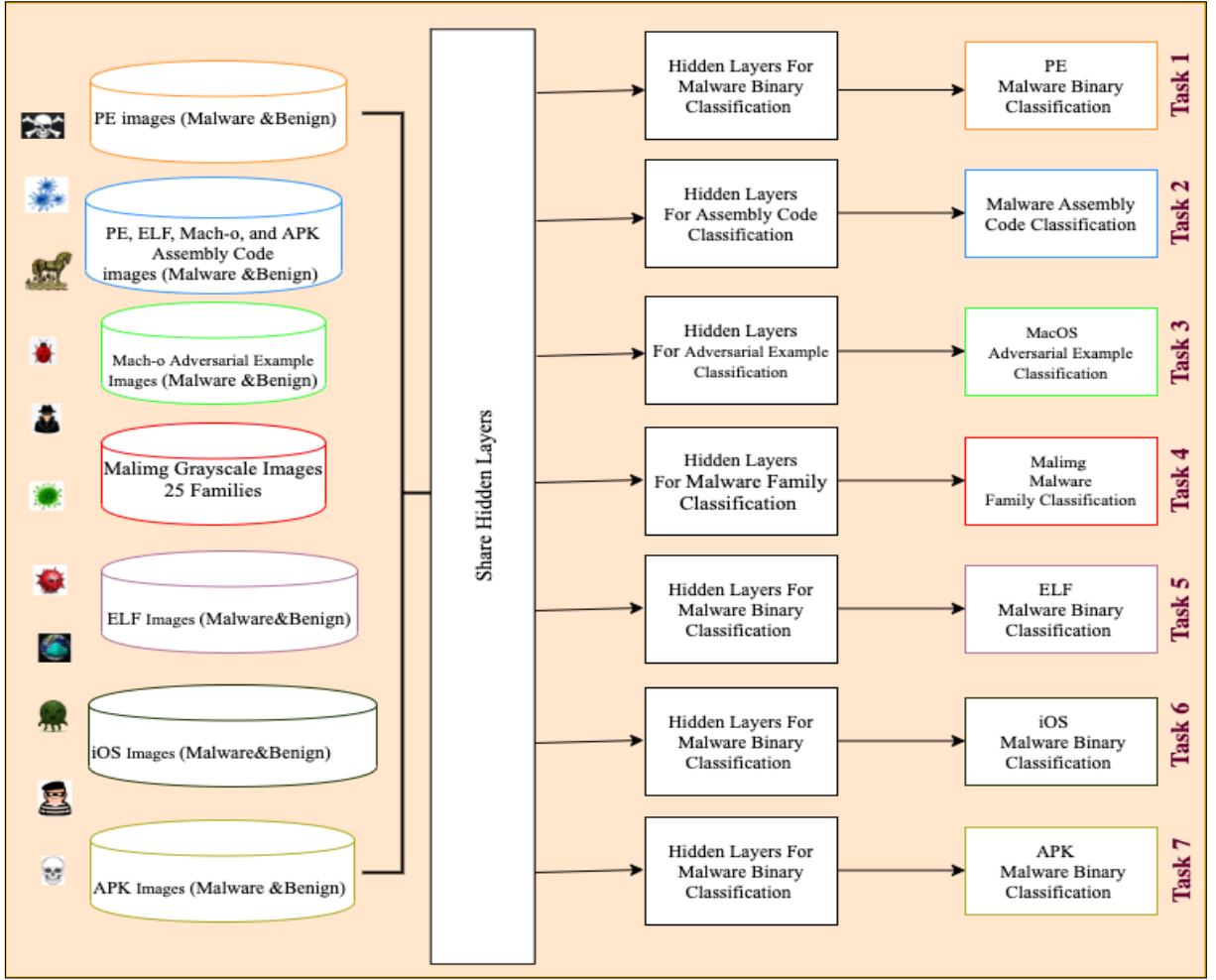


Figure 13: Our multi-task learning model

6.2.3. Parametric Rectified Linear Units (PReLU)

He et al. [50] proposed the parametric linear rectified (PReLU) to improve model fitting with nearly zero extra computational cost and little overfitting risk. In PReLU, the slope of negative part is learned from data instead of designing it as zero in ReLU. PReLU also generalizes the fixed small number used in LeakyReLU. PReLUs was shown to perform better than ReLU in a large scale image classification task [51]. The function is defined as:

$$f(x) = \begin{cases} a_i x & \text{for } x \leq 0, \\ x & \text{for } x > 0. \end{cases}$$

where i is the index of a channel and a_i is a learnable parameter.

6.2.4. Exponential linear unit (ELU)

The Exponential Linear Unit (ELU) is based on ReLU. It reduces the bias shift effect, and pushes the negative inputs to be close to zero [52]. It also speeds up learning, leading to better classification accuracy. ELU is defined as:

$$f(x) = \begin{cases} \alpha(\exp(x) - 1) & \text{for } x \leq 0, \\ x & \text{for } x > 0. \end{cases}$$

We used ELU in our experiments since it has achieved best published result on CIFAR-10 and CIFAR-100 [53]

6.3. Optimization

An optimizer is used in training to minimize the loss and to make our prediction as accurate as possible. Most deep learning models use stochastic gradient descent (SGD) [54]. Many adaptive variants of SGD have been invented, including Adam [55], Adagrad [56], Adadelta [57], RMSprop [58], and Nadam [59]. These five optimizers are used separately in our experiments, producing different results with our model as shown in Table 1. Among these adaptive optimizers, the Adam optimizer achieved the best performance. In summary, we compared four activation functions and five optimizers. The best performing activation function was PReLU and the best performing optimizer was Adam. On the other hand, the worst performing activation function was ReLU and the worst performing optimizer was Adadelta.



Figure 14: Our MTL model in detail

Table 1
Comparing five optimizers on the model.

Optimizer	Average Accuracy
Adam [55]	99.97%
Adagrad [56]	64.36%
Adadelta [57]	53.12%
RMSprop [58]	58.94%
RESprop [58]	60.43%

7. Datasets

We built several benchmark color Bitmap and JPG image datasets for Windows, Android, Linux, MacOS, and iOS operating systems of various malware executable files. The dataset samples were collected from VirusShare by BitTorrent⁹ that contains APKs, ELF, EXEs, and DLLs from May 2019 to Sep 2020. Mach-o and IPAs

samples were collected from VirusTotal and Contagio websites from Jun 2018 to Nov 2020.

Seven malware datasets were used in the experiments. The first one is a PE malware and benign color image dataset. The second dataset is the Mach-o Adversarial example malware and benign color image dataset. The third dataset is the ELF malware and benign color image dataset. The fourth dataset is Assembly code from PE, ELF, Mach-o, and APK malware and benign image dataset. The fifth dataset is a APK malware and benign color image dataset. The sixth dataset is a Mach-o and iOS malware and benign color image dataset. The seventh dataset is the Malimg grayscale image dataset [9] which contains 9339 malware images belonging to 25 different malware families. This dataset is publicly available.

We show a set of images obtained from malicious PE, Android, ELF, Mac, iOS samples. For instance, Fig. 15 shows the images for 8 different malicious samples.

⁹<https://www.bittorrent.com>

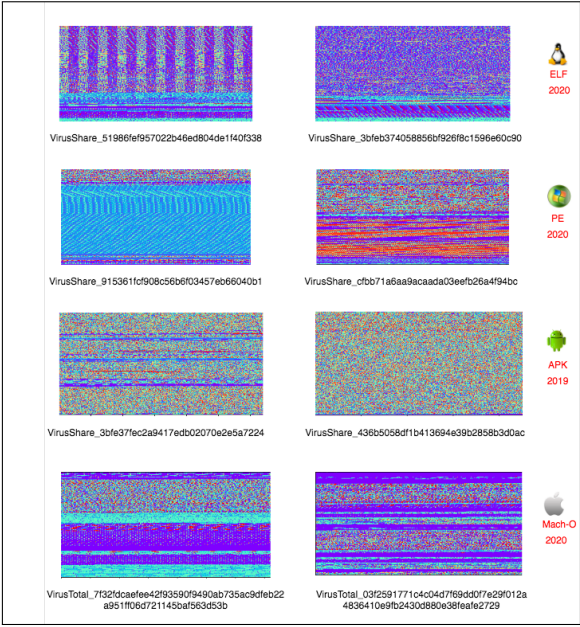


Figure 15: Malware samples from different operating systems

8. Evaluation

We evaluate the our model’s capability by using the following performance metrics: True Positive Rate (TPR), False Positive Rate (FPR) and Accuracy. TPR is the rate of malware samples correctly classified. FPR is the rate of malware samples falsely classified.

$$TPR(Recall) = \frac{TP}{TP + FN}$$

$$Precision = \frac{TP}{TP + FP}$$

$$Accuracy = \frac{TP + TN}{TP + FN + FP + TN}$$

$$F\text{-measure} = \frac{2 \times (Recall \times Precision)}{(Precision + Recall)}$$

$$ErrorRate = \frac{(FP + FN)}{(TP + TN + FP + FN)}$$

We repeated testing our model 5 times, and got the results as they are shown in Table 4. The accuracy of our model was between 99.80% – 99.97%, and the average accuracy was 99.91%, with the highest accuracy of 99.97%.

Fig. 16 and Fig. 17 show the confusion matrix for all tasks for predicting the classes of the examples in the testing dataset. All confusion matrices show superior performance on the diagonal. In Fig. 17, in the confusion matrix for task4, we observe that there is little misclassification and negligible errors, which means that classes close to the diagonal line have almost no similarities with other samples. As exception, the Lolyada.AA1 malware family has similarities with Lolyada.AA3 and Swizzor.gen!l with Swizzor.gen!E as well. These malware families have a little similarity behaviors.

We also test our model for binary classification of

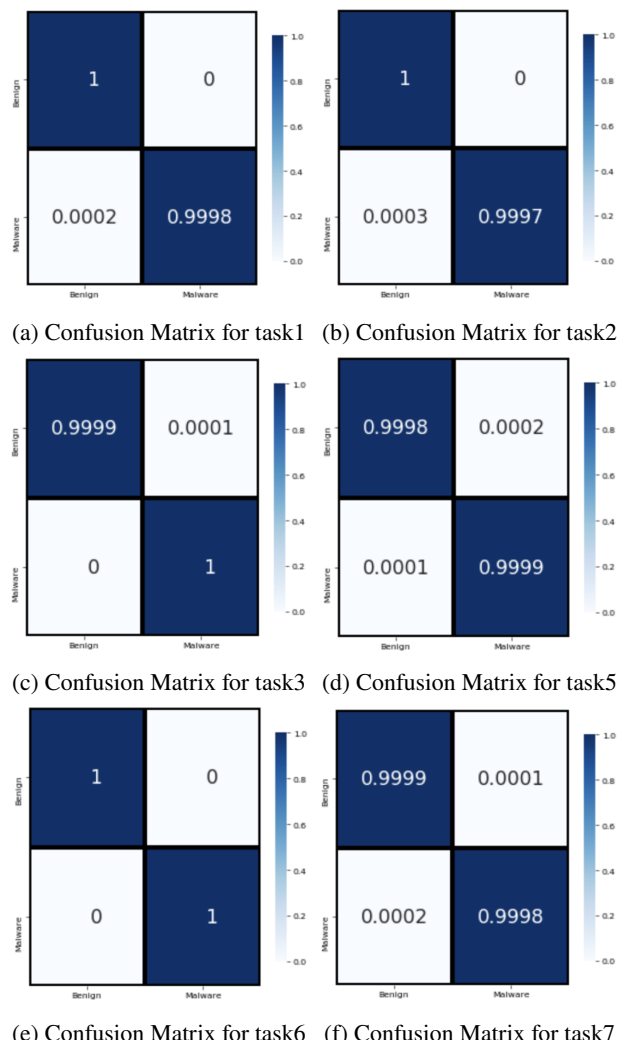


Figure 16: Confusion Matrix for malware image binary classification

malware versus benign in task1, task2, task3, task5, task6, and task 7. The confusion matrices for all these tasks are given in Figure 16.

9. Experimental Setup

We implemented the model using TensorFlow. The experiments were conducted on Google Colaboratory (also known as Colab). Google Colab is an execution environment that allows developers to write, run, and share code within Google Drive. Our datasets were mounted to the Google Colab using Google Drive. We used Python 3 with deep learning libraries and the model trained for about 8 hours. Our experimental results are illustrated in Table2 and Table3. One can see that our deep multi-task learning method has achieved competitive results.

9.1. Experimental Results

We evaluated our model performance and compared it with several other models. We show that multi-task learning can give a significant decrease in classification error. The training errors of four activation func-

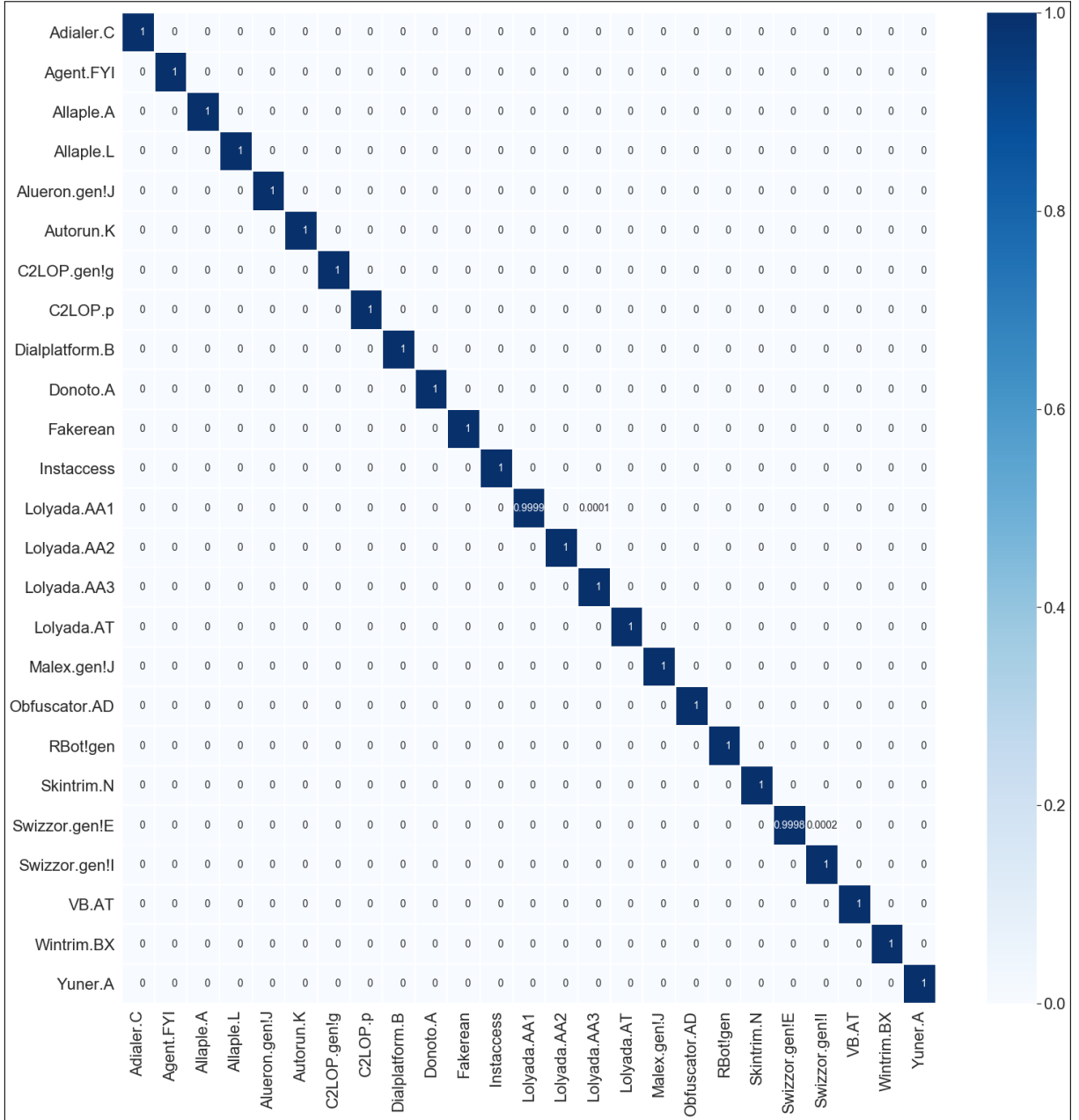


Figure 17: Confusion matrix for malware family classification-task4

tions were measured. Fig. 18 shows the testing error rates using our datasets. Fig. 19 shows that accuracy of PReLU is better than the other functions for training. In Fig. 20, the accuracies for PReLU, LeakReLU, and ELU are 99.97%, 99.91%, and 98.57%, respectively, while ReLU achieves 93.61% accuracy. We also compared the performance of the model with the existing deep learning approaches based on testing accuracy using the Malimg benchmark dataset, as shown in Table 2. Among the four activation functions, the PReLU had the lowest training error rate of 0.0003 and lowest test error rate of 0.0005 while ReLU had the highest training error rate 0.0017, and highest test error rate 0.0027 as shown in Table 3. The model performed best when using the PReLU activation function. Fig. 17 shows the testing error rates for the four activation functions.

The PReLU activation function is faster than the other activation functions with the lowest error rate. Fig. 18 shows the average accuracy of each activation function on all seven tasks. For the malware image binary classification task1, we obtain an accuracy of 99.88%, 99.94% for task2, 99.91% for task3, 99.89% for task5, 99.92% for task6, and 99.95% for task7, while task4 for the malware family classification yields a classification accuracy of 99.97% as shown in Table 5. Fig. 16 shows the confusion matrix for malware image binary classification for task1, task2, task3, task5, task6, and task7.

We conclude that the use of PReLU gives better performance than using other activation functions. In addition, most research on malware image classification converts malware into gray scale images. We demonstrate that color images are more effective in malware

image classification. Our study also has shown that using multi-task learning on malware images achieves the currently highest accuracy rate in malware image classification.

In addition, after trained combination all seven tasks $\{\tau_1, \tau_2, \tau_3, \tau_4, \tau_5, \tau_6, \tau_7\}$ we tested 900 samples of malware obfuscation that use various techniques on selected individual tasks $\{\tau_1\}, \{\tau_2\}, \{\tau_3\}, \{\tau_4\}, \{\tau_5\}, \{\tau_6\}, \{\tau_7\}$ they effectively detect all malware obfuscated techniques. Therefore, there is no impact of malware obfuscation on our model. Table 6 shows the number of samples for each malware obfuscation techniques that we tested. In table 5 we randomly choose multiple different tasks for testing together to see how to improve the testing accuracy and comparing with testing accuracy of each single task. For example, the accuracy of $\{\tau_1, \tau_2\}$ is more than $\{\tau_1\}$ and $\{\tau_2\}$ separately, also the accuracy of $\{\tau_1, \tau_2, \tau_3, \tau_4\}$ is more than $\{\tau_1, \tau_2, \tau_4\}$. We find that training more task together is improve the accuracy. However, experimental evaluation on seven tasks malware image classification trained by the MTL improves learning performance rather than single-task learning (STL) approach by 3.32%, as shown in table 5. For comparison between our model and the state-of-the-art approaches is given in Table 7. Note that Task 3 and Task 6 are shown that no comparison with the state-of-the-art since the iOS and MacOS malware classification uncovered research using images.

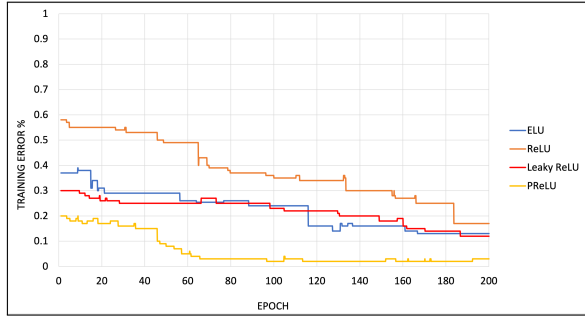


Figure 18: Testing error rates for four activation function

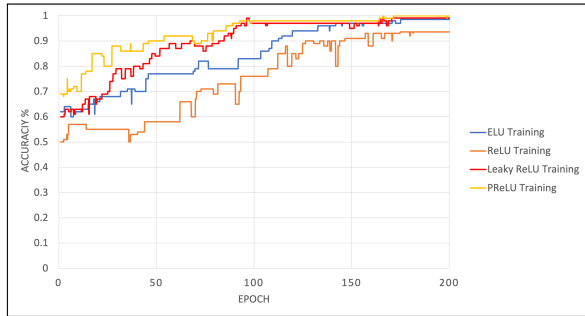


Figure 19: The accuracy during training for each activation function

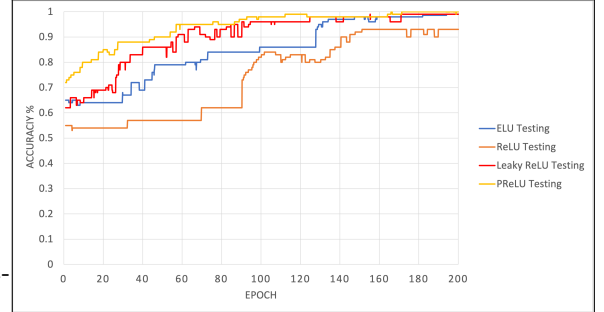


Figure 20: The accuracy during testing for each activation function

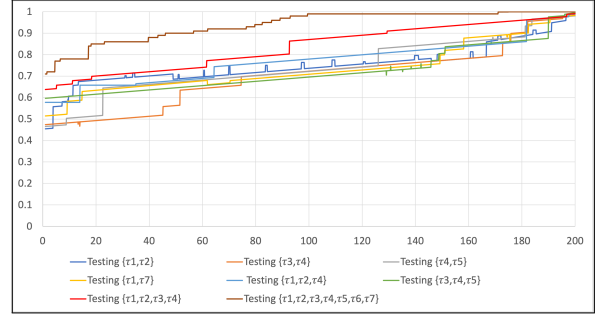


Figure 21: Testing accuracy on different tasks

10. Conclusions and Future Work

We proposed a novel method in this paper to detect malware by building a multi-task learning model and creating malware images. First, we generated images from various malware files for several operating systems: Android, Windows, MacOS, iOS, and Linux. We provided experimental results showing that our model can learn flexible shared parameters for related tasks, resulting in significantly improved performance over the state-of-the-art in malware image classification. In addition, our experiments show that the PReLU activation function has better generalization performance than ELU, ReLU, and LeakyReLU in our model with 11 layers. Training for 11 layers required 175 epochs to give best accuracy for all tasks. If we have than 11 layers the model needs more than 250 epochs.

The focus of future work is to use unrelated tasks like assembly code text and API calls text with our model to see if it hurts or improves performance of our model.

Table 2

Comparison between the average accuracy of the proposed model and some state-of-the-art models.

Method	Dataset images	Files	Accuracy
IDA+DRBA [60]	Malimg	PE	94.50%
GIST + KNN [60]	Malimg	PE	91.90%
GIST + SVM [60]	Malimg	PE	92.20%
GLCM + KNN [60]	Malimg	PE	92.50%
GLCM + SVM [60]	Malimg	PE	93.20%
VGG16 + Softmax [60]	Malimg	PE	90.77%
VGG16 + SVM [61]	Malimg	PE	92.97%
Light-weight DL [11]	Malimg	PE	94.00%
NSGA-II [62]	Malimg	PE	97.60%
ResNet + Sofrmax [63]	Malimg	PE	98.62%
IMCEC [10]	Malimg	PE	99.50%
IMCFN [64]	RGB Malimg	PE	98.82%
Vgg-verydeep-19 [65]	Malimg	PE	97.18%
Custom CNN [66]	Malimg	PE	98.48%
Custom CNN [66]	Microsoft malware	PE	97.49%
VisDroid [67]	Android Drebin	APK	98.14%
Random Forest [68]	Android Drebin	APK	95.42%
Inception V3 [13]	Malimg	PE	99.24%
Our multi-task learning model	Malimg + Malware color images	PE + ELF + APK + Mach-o	99.97%

Table 3

Error rate for four different activation functions.

Activation	Training Error	Test Error
ReLU	0.0017	0.0027
Leaky ReLU	0.0012	0.0022
ELU	0.0013	0.0021
PReLU	0.0003	0.0005

Table 4

Testing the model 5 times.

No	Accuracy (%)	TPR (%)	FPR (%)
1	99.87	99.88	0.45
2	99.90	99.92	0.50
3	99.91	99.93	0.65
4	99.94	99.95	0.66
5	99.97	99.98	0.73

References

- [1] J. D. McAfee, Malware Threats Statistics, 2020.
- [2] D. Ucci, L. Aniello, R. Baldoni, Survey of machine learning techniques for malware analysis, *Computers & Security* 81 (2019) 123–147.
- [3] M. K. Alzaylae, S. Y. Yerima, S. Sezer, Di-droid: Deep learning based android malware detection using real devices, *Computers & Security* 89 (2020) 101663.
- [4] H. Darabian, S. Homayounoot, A. Dehghantanha, S. Hashemi, H. Karimipour, R. M. Parizi, K.-K. R. Choo, Detecting cryptomining malware: a deep learning approach for static and dynamic analysis, *Journal of Grid Computing* (2020) 1–11.
- [5] A. Souris, N. J. Navimipour, A. M. Rahmani, Formal verification approaches and standards in the cloud computing: a comprehensive and systematic review, *Computer Standards & Interfaces* 58 (2018) 1–22.
- [6] V. Sihag, M. Vardhan, P. Singh, A survey of android application and malware hardening, *Computer Science Review* 39 (2021) 100365.
- [7] J. Qiu, J. Zhang, W. Luo, L. Pan, S. Nepal, Y. Xiang, A survey of android malware detection with deep neural models, *ACM Computing Surveys (CSUR)* 53 (2020) 1–36.
- [8] Q.-D. Ngo, H.-T. Nguyen, V.-H. Le, D.-H. Nguyen, A survey of iot malware and detection methods based on static features, *ICT Express* 6 (2020) 280–286.
- [9] L. Nataraj, S. Karthikeyan, G. Jacob, B. S. Manjunath, *Malware Images: Visualization and Automatic classification*, 2011.
- [10] D. Vasan, M. Alazab, S. Wassan, B. Safaei, Q. Zheng, Image-Based Malware Classification Using Ensemble of CNN Architectures (IMCEC), *Computers & Security* (2020) 101748.
- [11] J. Su, V. D. Vasconcellos, S. Prasad, S. Daniele, Y. Feng, K. Sakurai, Lightweight Classification of IoT Malware Based on Image Recognition, 2018.
- [12] S. Ni, Q. Qian, R. Zhang, Malware Identification using Visualization Images and Deep Learning, *Computers & Security* 77 (2018) 871–885.
- [13] A. Bensaoud, N. Abudawood, J. Kalita, Classifying malware images with convolutional neural network models, *International Journal of Network Security* 22 (2020) 1022–1031.
- [14] H. Naeem, F. Ullah, M. R. Naeem, S. Khalid, D. Vasan, S. Jabbar, S. Saeed, Malware detection in industrial internet of things based on hybrid image visualization and deep learning model, *Ad Hoc Networks* (2020) 102154.
- [15] M. Kalash, M. Rochan, N. Mohammed, N. D. Bruce, Y. Wang, F. Iqbal, Malware classification with deep convolutional neural networks, 2018.
- [16] F. Mercaldo, A. Santone, Deep learning for image-based mobile malware detection, *Journal of Computer Virology and Hacking Techniques* (2020) 1–15.
- [17] E. Meyerson, R. Miikkulainen, Pseudo-task augmentation: From deep multitask learning to intratask sharing—and back, *arXiv preprint arXiv:1803.04062* (2018).
- [18] K. Zhang, L. Zheng, Z. Liu, N. Jia, A deep learning based multitask model for network-wide traffic speed prediction, *Neurocomputing* 396 (2020) 438–450.
- [19] G. Gkioxari, B. Hariharan, R. Girshick, J. Malik, R-cnns for Pose Estimation and Action Detection, *arXiv preprint arXiv:1406.5212* (2014).
- [20] J. Zhao, Y. Peng, X. He, Attribute hierarchy based multi-task learning for fine-grained image classification, *Neurocomputing* 395 (2020) 150–159.
- [21] C. Wah, S. Branson, P. Welinder, P. Perona, S. Belongie, The

Table 5

Comparison the testing among all tasks results.

Tasks	$\{\tau_1\}$	$\{\tau_2\}$	$\{\tau_3\}$	$\{\tau_4\}$	$\{\tau_5\}$	$\{\tau_6\}$	$\{\tau_7\}$
$\{\tau_1\}$	96.56%						
$\{\tau_2\}$		97.02%					
$\{\tau_3\}$			96.89%				
$\{\tau_4\}$				97.86%			
$\{\tau_5\}$					96.67%		
$\{\tau_6\}$						96.11%	
$\{\tau_7\}$							96.84%
$\{\tau_1, \tau_2\}$	98.36%	97.56%					
$\{\tau_3, \tau_4\}$			98.12%	98.72%			
$\{\tau_4, \tau_5\}$				98.80%	98.45%		
$\{\tau_1, \tau_7\}$	98.02%						98.39%
$\{\tau_1, \tau_2, \tau_4\}$	99.10%	99.12%			99.03%		
$\{\tau_3, \tau_4, \tau_5\}$			99.05%	99.24%	99.15%		
$\{\tau_1, \tau_2, \tau_3, \tau_4\}$	99.19%	99.22%	99.20%	99.17%			
$\{\tau_1, \tau_2, \tau_3, \tau_4, \tau_5, \tau_6, \tau_7\}$	99.88%	99.94%	99.91%	99.97%	99.89%	99.92%	99.95%

Table 6

Malware Obfuscation techniques.

#	Obfuscation Techniques	Samples
1	Disassembling & Reassembling	50
2	Changing Package Name	100
3	Repacking	60
4	Identifier Renaming	40
5	Call Indirections	55
6	Junk Code Insertion	30
7	Garbage Code Insertion	100
8	Register Usage Exchange	70
9	Instruction replacement	35
10	Dead code insertion	40
11	Register reassignment	60
12	Subroutine Permutation	50
13	Code transposition	70
14	Code Reordering through Jump Instruction	60
15	Code integration (Zmist)	80

Table 7

Comparing with the state-of-the-art methods for each task.

Tasks	Accuracy	Models	Accuracy
τ_1	99.88%	MSIC [69]	96%
τ_2	99.94%	Khan et al. [70]	88.36%
τ_3	99.91%	-	-
τ_4	99.97%	IMCFN [64]	98.27%
τ_5	99.89%	Su et al. [71]	94%
τ_6	99.92%	-	-
τ_6	99.95%	IMCFN [64]	97.35%

caltech-ucsd birds-200-2011 dataset (2011).

[22] J. Krause, M. Stark, J. Deng, L. Fei-Fei, 3d object representations for fine-grained categorization, in: Proceedings of the IEEE international conference on computer vision workshops, 2013, pp. 554–561.

[23] S. Bell, Y. Liu, S. Alsheikh, Y. Tang, E. Pizzi, M. Henning, K. Singh, O. Parkhi, F. Borisyuk, Groknet: Unified computer vision model trunk and embeddings for commerce, 2020.

[24] F. Yu, H. Chen, X. Wang, W. Xian, Y. Chen, F. Liu, V. Madhava, T. Darrell, Bdd100k: A diverse driving dataset for heterogeneous multitask learning, 2020.

[25] Z. Chen, R. Wang, M. Yu, H. Gao, Q. Li, H. Wang, Spatial-temporal multi-task learning for salient region detection, Pattern Recognition Letters 132 (2020) 76–83.

[26] X. Wang, H. Chen, A.-R. Ran, L. Luo, P. P. Chan, C. C. Tham, R. T. Chang, S. S. Mannil, C. Y. Cheung, P.-A. Heng, Towards multi-center glaucoma ocl image screening with semi-supervised joint structure and function multi-task learning, Medical Image Analysis 63 (2020) 101695.

[27] M. Dorado-Moreno, N. Navarin, P. A. Gutiérrez, L. Prieto, A. Sperduti, S. Salcedo-Sanz, C. Hervás-Martínez, Multi-task learning for the prediction of wind power ramp events with deep neural networks, Neural Networks 123 (2020) 401–411.

[28] U. Drepper, How to Write Shared Libraries, Retrieved Jul 16 (2006) 2009.

[29] H. Choi, B. B. Zhu, H. Lee, Detecting Malicious Web Links and Identifying Their Attack Types., WebApps 11 (2011) 218.

[30] AppNee, PEiD - Popular PE Packer /Cryptor/Compiler Detector, 2020.

[31] J. Smart, S. Csomor, et al., Cross-Platform GUI Programming with wxWidgets, Prentice Hall Professional, 2005.

[32] I. Goodfellow, J. Pouget-Abadie, M. Mirza, B. Xu, D. Warde-Farley, S. Ozair, A. Courville, Y. Bengio, Generative adversarial nets, in: Advances in neural information processing systems, 2014, pp. 2672–2680.

[33] T. Karras, S. Laine, T. Aila, A style-based generator architecture for generative adversarial networks, in: Proceedings of the IEEE/CVF Conference on Computer Vision and Pattern Recognition, 2019, pp. 4401–4410.

[34] A. Brock, J. Donahue, K. Simonyan, Large scale gan training for high fidelity natural image synthesis, arXiv preprint arXiv:1809.11096 (2018).

[35] Z. Zhang, Y. Xie, L. Yang, Photographic text-to-image synthesis with a hierarchically-nested adversarial network, in: Proceedings of the IEEE Conference on Computer Vision and Pattern Recognition, 2018, pp. 6199–6208.

[36] C. Ledig, L. Theis, F. Huszár, J. Caballero, A. Cunningham, A. Acosta, A. Aitken, A. Tejani, J. Totz, Z. Wang, et al., Photo-Realistic Single Image Super-Resolution Using a Generative Adversarial Network, 2017.

[37] P. Isola, J.-Y. Zhu, T. Zhou, A. A. Efros, Image-to-Image Translation with Conditional Adversarial Networks, ????

[38] J.-Y. Zhu, T. Park, P. Isola, A. A. Efros, Unpaired Image-to-Image Translation Using Cycle-Consistent Adversarial Networks, 2017.

[39] T. Kim, M. Cha, H. Kim, J. K. Lee, J. Kim, Learning to Discover Cross-Domain Relations with Generative Adversarial

Networks, arXiv preprint arXiv:1703.05192 (2017).

[40] Z. Yi, H. Zhang, P. Tan, M. Gong, Dualgan: Unsupervised Dual Learning for Image-to-Image Translation, ????

[41] Y. Choi, M. Choi, M. Kim, J.-W. Ha, S. Kim, J. Choo, Stargan: Unified Generative Adversarial Networks for Multi-Domain Image-to-Image translation, 2018.

[42] C. Szegedy, W. Liu, Y. Jia, P. Sermanet, S. Reed, D. Anguelov, D. Erhan, V. Vanhoucke, A. Rabinovich, Going deeper with convolutions, in: Proceedings of the IEEE conference on computer vision and pattern recognition, 2015, pp. 1–9.

[43] K. Simonyan, A. Zisserman, Very deep convolutional networks for large-scale image recognition, arXiv preprint arXiv:1409.1556 (2014).

[44] K. He, X. Zhang, S. Ren, J. Sun, Deep residual learning for image recognition, in: Proceedings of the IEEE conference on computer vision and pattern recognition, 2016, pp. 770–778.

[45] H. Gao, H. Yuan, Z. Wang, S. Ji, Pixel transposed convolutional networks, IEEE transactions on pattern analysis and machine intelligence 42 (2019) 1218–1227.

[46] G. Huang, Z. Liu, L. Van Der Maaten, K. Q. Weinberger, Densely connected convolutional networks, in: Proceedings of the IEEE conference on computer vision and pattern recognition, 2017, pp. 4700–4708.

[47] V. Nair, G. E. Hinton, Rectified Linear Units Improve Restricted Boltzmann Machines, 2010.

[48] A. L. Maas, A. Y. Hannun, A. Y. Ng, Rectifier NONLINEarities Improve Neural Network Acoustic Models, 2013.

[49] S. Mastromichalakis, Alrelu: A different approach on leaky relu activation function to improve neural networks performance, arXiv preprint arXiv:2012.07564 (2020).

[50] K. He, X. Zhang, S. Ren, J. Sun, Delving Deep into Rectifiers: Surpassing Human-Level Performance on Imagenet classification, 2015.

[51] S.-H. Wang, K. Muhammad, J. Hong, A. K. Sangaiah, Y.-D. Zhang, Alcoholism identification via convolutional neural network based on parametric relu, dropout, and batch normalization, Neural Computing and Applications 32 (2020) 665–680.

[52] D.-A. Clevert, T. Unterthiner, S. Hochreiter, Fast and Accurate Deep Network Learning by Exponential Linear Units (elus), arXiv preprint arXiv:1511.07289 (2015).

[53] M. Z. Alom, M. Hasan, C. Yakopcic, T. M. Taha, V. K. Asari, Improved inception-residual convolutional neural network for object recognition, Neural Computing and Applications 32 (2020) 279–293.

[54] S. Ruder, An overview of gradient descent optimization algorithms, arXiv preprint arXiv:1609.04747 (2016).

[55] D. P. Kingma, J. Ba, Adam: A Method for Stochastic Optimization, arXiv preprint arXiv:1412.6980 (2014).

[56] J. Duchi, E. Hazan, Y. Singer, Adaptive subgradient methods for online learning and stochastic optimization., Journal of machine learning research 12 (2011).

[57] M. D. Zeiler, Adadelta: an adaptive learning rate method, arXiv preprint arXiv:1212.5701 (2012).

[58] N. Loizou, P. Richtárik, Momentum and stochastic momentum for stochastic gradient, newton, proximal point and subspace descent methods, Computational Optimization and Applications 77 (2020) 653–710.

[59] T. Dozat, Incorporating nesterov momentum into adam (2016).

[60] Z. Cui, F. Xue, X. Cai, Y. Cao, G.-g. Wang, J. Chen, Detection of Malicious Code Variants Based on Deep Learning, IEEE Transactions on Industrial Informatics 14 (2018) 3187–3196.

[61] E. Rezende, G. Ruppert, T. Carvalho, A. Theophilo, F. Ramos, P. de Geus, Malicious Software Classification using VGG16 Deep Neural Network’s Bottleneck Features, in: Information Technology-New Generations, Springer, 2018, pp. 51–59.

[62] Z. Cui, L. Du, P. Wang, X. Cai, W. Zhang, Malicious Code Detection Based on CNNs and Multi-Objective Algorithm, Journal of Parallel and Distributed Computing 129 (2019) 50–58.

[63] E. Rezende, G. Ruppert, T. Carvalho, F. Ramos, P. De Geus, Malicious Software Classification using Transfer Learning of Resnet-50 Deep Neural Network, 2017.

[64] D. Vasan, M. Alazab, S. Wassan, H. Naeem, B. Safaei, Q. Zheng, IMCFN: Image-Based Malware Classification using Fine-Tuned Convolutional Neural Network architecture, Computer Networks 171 (2020) 107138.

[65] S. Yue, Imbalanced Malware Images Classification: a CNN Based approach, arXiv preprint arXiv:1708.08042 (2017).

[66] D. Gibert, C. Mateu, J. Planes, R. Vicens, Using Convolutional Neural Networks for Classification of Malware Represented as Images, Journal of Computer Virology and Hacking Techniques 15 (2019) 15–28.

[67] K. Bakour, H. M. Ünver, VisDroid: Android Malware Classification Based on Local and Global Image Features, Bag of Visual Words and Machine Learning Techniques, Neural Computing and Applications (2020) 1–21.

[68] M. Yang, Q. Wen, Detecting Android Malware by Applying Classification Techniques on Images Patterns, 2017.

[69] A. Azab, M. Khasawneh, Msic: Malware spectrogram image classification, IEEE Access 8 (2020) 102007–102021.

[70] R. U. Khan, X. Zhang, R. Kumar, Analysis of resnet and googlenet models for malware detection, Journal of Computer Virology and Hacking Techniques 15 (2019) 29–37.

[71] J. Su, D. V. Vasconcellos, S. Prasad, D. Sgandurra, Y. Feng, K. Sakurai, Lightweight classification of iot malware based on image recognition, in: 2018 IEEE 42nd Annual Computer Software and Applications Conference (COMPSAC), volume 02, 2018, pp. 664–669. doi:10.1109/COMPSAC.2018.10315.